JOURNAL OF COLLOID AND INTERFACE SCIENCE 164, 21–34 (1994)

Effects of Ionic Strength and Flow Rate on Colloid Release: Relating Kinetics to Intersurface Potential Energy

JOSEPH N. RYAN

Department of Civil, Environmental, and Architectural Engineering, Campus Box 428, University of Colorado, Boulder, Colorado 80309

AND

PHILIP M. GSCHWEND

Division of Water Resources and Environmental Engineering, Department of Civil and Environmental Engineering, Massachusetts Institute of Technology 48-415, Cambridge, Massachusetts 02139

Received August 26, 1992; accepted October 22, 1993

The effects of ionic strength and flow rate on the release of hematite colloids from quartz surfaces were observed in a packed bed column. The rates of colloid release, prompted by an abrupt increase in solution pH, increased as ionic strength was decreased; however, the corresponding intersurface potential energy barriers, calculated using extended DLVO theory and a Born repulsion collision parameter of $\sigma = 5$ Å, increased in size. Furthermore, the observed release rates increased with increasing flow rate. These results suggest that colloid transport "over an energy barrier" was not the rate-limiting step in these experiments. We hypothesized that the increase in solution pH was sufficient to cause the disappearance of the detachment energy barrier in these experiments. When we calculated the double layer potentials with surface potentials (estimated using a surface complexation–double layer model) instead of zeta potentials (which decrease with increasing ionic strength owing to compression of the double layer), the potential energy profiles still contained energy barriers. To force removal of the energy barriers in the calculated potential energy profiles, we increased the short-range repulsive energy by increasing the Born collision parameter from 5 to 20 Å, resulting in effective distances of closest approach of about 7 Å. This change resulted in correspondence of the trends in the observed and predicted detachment behavior. In the absence of an energy barrier, we hypothesized that colloid transport across a diffusion boundary layer would control the rate of colloid release. In this case, the colloid release rate should be related to the flow rate through the influence of the flow rate on the thickness of the diffusion boundary layer. The observed dependence of the release rates on the estimated boundary layer thickness was close to that predicted for the release rate–boundary layer thickness relationship.

INTRODUCTION

The release of colloids from surfaces is a concern in many fields, including wastewater filtration, subsurface transport of viruses and bacteria, and enhanced transport of colloid-associated contaminants in groundwater. The transport of low-solubility contaminants that readily associate with colloids (e.g., radionuclides and trace metals) has been documented in a number of aquifers (1–4); however, the source of the colloids responsible for transport has not always been investigated. In groundwater, colloids may be formed by precipitation of supersaturated phases (5, 6), erosion of secondary minerals from fractures (7), dissolution of cementing minerals (8, 9), or changes in solution ionic strength and pH (10, 11).

Changes in solution ionic strength (I) and pH affect the electrostatic interactions between colloid and grain surfaces. These interactions have been described by the DLVO theory (12, 13) as the sum of the double layer and London–van der Waals potential energies over the distance separating the surfaces. Additionally, a term accounting for the short-range repulsion between surfaces is often included to prevent colloid-grain interpenetration (14, 15). The effects of variations in the intersurface potential energy on colloid release have been modeled by relating the rate of colloid detachment to the size of the potential energy barrier opposing detachment in an Arrhenius relationship (16–18). According to this energy barrier model, the rates of colloid attachment and detachment are exponentially related to the sizes of the energy barrier opposing attachment ($-[\phi_{max}]$) and detachment ($-[\phi_{max} - \phi_{min1}]$). Colloid diffusive transport over these energy barriers is the rate-limiting step in attachment and detachment (Fig. 1, Case B). However, deposition rates predicted using the attachment energy barrier are typically orders of magnitude lower than measured deposition rates (19–22). In contrast, Kallay *et al.* (23) summarized the results of a series of colloid release experiments in which the observed rates corresponded well with predicted rates estimated with DLVO theory and adjustable distances of closest approach of colloids to surfaces.

0021-9797/94 $6.00

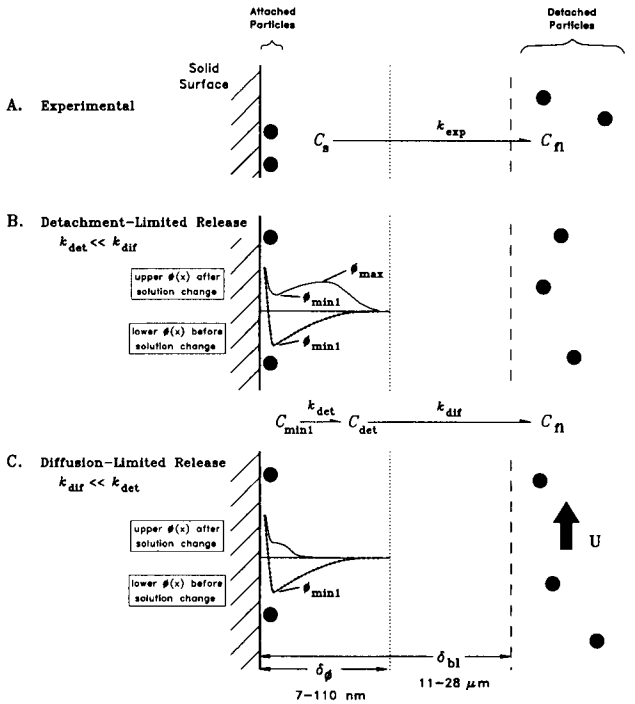

FIG. 1. Schematics of experimental, detachment-limited, and diffusion-limited colloid release from surfaces. When the thickness of the hydrodynamic boundary layer (δ_{bl}) is much greater than the thickness of the region influenced by the intersurface potential energy (δ_ϕ), colloid release is postulated to be a two-step mechanism in which either detachment from the surface or diffusion across the boundary layer can control the overall release rate. The overall release rate is defined by the experimentally observed (Case A) colloid surface concentration (C_s), first order release rate coefficient (k_{exp}), and colloid concentration in the bulk fluid (C_{fl}) moving with velocity U. Detachment-limited (Case B) and diffusion-limited (Case C) release are defined by the concentration of colloids attached in the primary minimum (ϕ_{min1}) of the potential energy profile (C_{min1}), the concentration of colloids detached from the surface (C_{det}), the rate coefficient for detachment (k_{det}), and the rate coefficient for diffusion across δ_{bl} (k_{dif}). Colloid release is limited by detachment ($C_{min1} \rightarrow C_{det}$) when the potential energy barrier ($[-(\phi_{max} - \phi_{min1})]$, where ϕ_{max} is the primary maximum of potential energy), is present and by diffusion ($C_{det} \rightarrow C_{fl}$) when the energy barrier is removed by a change in solution chemistry.

In the field, we have observed the mobilization of clay colloids in an iron-oxide-coated sand aquifer affected by infiltration of organic matter-rich, anoxic groundwater (24, 25). Recently, we measured the rates of clay colloid release from laboratory columns containing iron-oxide-coated sand recovered from the field (26). The columns were subjected to solutions of varying ionic strength, pH, and ascorbate (an Fe(III) reductant) and dodecanoate (an anionic surfactant) concentrations. These experiments indicated that the release of the natural colloids was controlled by the changes in electrostatic interactions between colloid surfaces (goethite, kaolinite) resulting from perturbations of solution chemistry. For example, a decrease in I resulted in a slight increase in the colloid release rate because, at lower I, the repulsive double layers extend further into solution. In contrast, we found that energy barriers calculated using an extended DLVO theory were larger for lower I; thus, even the *trends* in the release rates in the experiment in which I was varied were not predicted by the energy barrier model.

A further complication in the effect of I on colloid detachment comes from the experiments summarized by Kallay *et al.* (23). In most of the experiments in which I was increased, colloid release rates decreased; however, Kallay *et al.* (27) observed an increase in release rate when I was increased in a system of hematite colloids and glass grains.

To assess these contradictory results, we experimentally re-examined the kinetics of hematite colloid detachment from quartz grains as a function of ionic strength. We also explored the effects of varying parameters in the calculation of the DLVO-based potential energy profile to seek insight into the correspondence of the energy barrier size with the experimental data. Finally, we varied the flow rate in our hematite–quartz system to test a hypothesis that transport of the detached colloids through the diffusion boundary layer was the rate-determining step in our observed colloid release (Fig. 1, Case C).

METHODS

Experimental

Materials. Detachment of hematite colloids from quartz grains was studied in a short, wide flow-through column. The spherical hematite colloids were prepared by aging a 0.018 M $FeCl_3$ and 0.001 M HCl solution made with 0.22 μm-filtered, distilled, deionized water (ddW, Millipore Milli-Q® system) at 100°C for 24 h (28) in polyethylene bottles and were stored at room temperature until used in the experiments. Prior to attachment to the quartz grains, aliquots of the stock suspension were rinsed with ddW until the pH of the suspension matched that of the ddW (pH 5.7 to 6.0). The rinsed colloids were stored in ddW overnight. The hydrodynamic size of the rinsed colloids was determined prior to each experiment by photon correlation spectroscopy (PCS; Coulter N4, Hialeah, FL). For all experiments, the mean and standard deviation of the colloid size was 150 ± 35 nm; for individual experiments, the standard deviation was always less than 10% of the mean. The isoelectric point of the hematite colloids in 1×10^{-3}, 1×10^{-2}, and 1×10^{-1} M $NaNO_3$ solutions was pH 8.0 ± 0.1, as determined by microelectrophoresis (Rank Bros. MkII, cylindrical cell, 3 mW He–Ne laser). Suspension concentrations were determined by light scattering at 90° (turbidimetry; Hach Ratio X/R). A linear relationship was observed between scattering intensity (NTU) and hematite colloid concentration (H; mg liter^{-1}) trapped on 0.02 μm Whatman Anodisc filters (H = 0.312 [NTU] − 0.00125; R^2 = 0.9973).

The subrounded quartz grains (Aldrich Chemical Co.,

Inc., 50 to 70 mesh) ranged from 210 to 300 μm in diameter. They were heated at 450°C for 6 h and soaked in 1.0 N HNO_3 overnight to remove organic matter and other surface impurities, rinsed with ddW until the pH of the suspension matched that of the ddW, and dried before the experiments.

Procedures. The hematite colloids were attached to the quartz grains by vigorously shaking 1.0 ml of the hematite suspension with 5.00 g quartz in 20 ml of a 1×10^{-4} *M* HNO_3 solution for 30 min. The hematite–quartz suspension was washed three times with the 1×10^{-4} *M* HNO_3 solution and stored 16 to 20 h in 1×10^{-4} *M* HNO_3 solution before the experiments. The hematite-coated quartz grains were transferred with ddW to a 47 mm Millipore Swinnex filter holder containing a 0.22 μm Millipore membrane filter and nylon screen (120 mesh) on the inlet end and a nylon screen on the outlet end. A 40 mm diameter Viton o-ring surrounded the grains.

Flushing solutions were purged with Ar prior to being adjusted to the proper pH and pumped upward through the quartz sand-filled column with a Milton Roy HPLC pump. The solution reservoir was flushed with Ar during the experiment. Experiments testing the deposition of hematite colloids onto uncoated quartz grains in the column showed that flow was evenly distributed across the diameter of the column.

In preliminary detachment tests, the amount of colloids removed from the column by flushing at 1.0 ml min^{-1} with pH 7.0 solutions of 1×10^{-4} and 1×10^{-3} *M* ionic strength was below the detection limit (~0.001 mg $liter^{-1}$). The pH and *I* were adjusted with NaOH and $NaNO_3$, respectively. Flushing with pH 10.0, $I = 1 \times 10^{-4}$ *M* solutions removed a maximum of only 1% of the total colloids. Thus, the remainder of the experiments were conducted at pH 11.0 to increase the colloid concentration in the eluent.

The flushing solution *I* was varied in the first detachment experiment (ΔI). Solutions of pH 11.0 and *I* from 1×10^{-3} to 1×10^{-1} *M* were run through columns at a flow rate of 1.0 ± 0.05 ml min^{-1}. Flow rate was varied in the second detachment experiment (ΔQ). Solutions of pH 11 (1×10^{-3} *M* NaOH) were pumped through the column at flow rates ranging from 0.51 to 11.7 ml min^{-1} (pore velocities of 1.5 to 34 m day^{-1}).

Column eluent samples were collected in glass vials. Aliquots of each sample were analyzed by PCS for colloid size in 60 s analyses. To measure the colloid concentration, the samples were diluted if necessary, inverted five times to mix, sonicated in an 80 W bath for 5 s to purge bubbles, and quantified by turbidity. The experiments were stopped when the scattering intensity of the eluent fell below that of 0.22 μm-filtered deionized water (0.030 ± 0.010 NTU).

The concentrations of hematite colloids remaining in the columns were measured by turbidity after the residual grains were twice sonicated in a polycarbonate tube filled with a known volume of 1×10^{-3} *M* NaOH solution for 10 min. The colloid concentration was corrected for the presence of quartz colloids suspended during sonication by subtracting the scattering intensity of quartz grain blanks. The amount of colloids remaining in the column plus the amount of those collected in the column eluent always matched the total amount of colloids added to the quartz grains to within 5%. After some experiments, residual grains coated with Au–Pd were examined by scanning electron microscopy and energy-dispersive X-ray spectroscopy (SEM/EDX; Cambridge Stereoscan 240, Link Analytical).

Detachment rate coefficients. The results of the colloid release experiments are expressed as the fraction of colloid mass remaining in the column at time *t* to initial total colloid mass ($[C_s]_t/[C_s]_0$). To account for the delay in colloid release caused by the presence of colloid-free water initially in the column, the experimental times were adjusted by subtracting the time required to flush one pore volume. The column pore volume was estimated as

$$V_{pore} = (h_{col}\pi R_{col}^2) - (m_g/\rho_g), \qquad [1]$$

where the column radius R_{col} was 2.0 cm, the column height h_{col} ranged from 0.25 to 0.30 cm, the mass of solid m_g was 5.00 g, and the quartz density ρ_g was taken as 2.65 g cm^{-3}. The experimental rate coefficients k_{exp} were determined by fitting the data by nonlinear least-squares regression to an exponential function (Table 1),

$$k_{exp} = -\frac{1}{t}\ln\left(\frac{[C_s]_t - [C_s]_{eq}}{[C_s]_0 - [C_s]_{eq}}\right). \qquad [2]$$

Calculation of Detachment Energies

Intersurface potential energy. The physical interactions between approaching colloid surfaces were expressed in terms of an augmented DLVO theory as the sum of the van der Waals, Born, and double layer potential energy varying with separation distance *x*:

$$\phi^{tot}(x) = \phi^{vdW}(x) + \phi^{Born}(x) + \phi^{dl}(x). \qquad [3]$$

The van der Waals potential, derived from the attractive term of the Lennard–Jones *m–n* interatomic potential with an x^{-6} dependence on separation distance, was formulated for unretarded sphere–sphere interaction by assuming pairwise additivity of the interatomic potentials (29),

$$\phi^{vdW} = -\frac{A_{132}}{12}\left\{\frac{y}{r^2 + ry + r} + \frac{y}{r^2 + ry + r + y} + 2\ln\left[\frac{r^2 + ry + r}{r^2 + ry + r + y}\right]\right\}, \qquad [4]$$

where $y = a_g/a_c$, $r = x/2a_c$, a_c and a_g are the colloid and grain radii, respectively, and A_{132} is the complex Hamaker

TABLE 1
Rate Coefficients and Total Fractions of Colloids Released in Hematite–Quartz ΔI and ΔQ and $Cr(OH)_3$–Glass ΔI Experiments

Colloid/grain/exp. (Ref.)	Ionic strength I (M)	Flow rate Q (ml min^{-1})	Fitted[a] rate coefficient k_{exp} (s^{-1})	Final fraction remaining	Fitted[a] fraction remaining C_{eq}
α-Fe_2O_3/quartz/ΔI (this study)	0.001	1.00 ± 0.03	$1.34 \pm 0.05 \cdot 10^{-3}$	0.948	0.949 ± 0.001
	0.003		$1.21 \pm 0.07 \cdot 10^{-3}$	0.957	0.957 ± 0.001
	0.01		$1.11 \pm 0.07 \cdot 10^{-3}$	0.972	0.973 ± 0.001
	0.03		$9.47 \pm 0.51 \cdot 10^{-4}$	0.989	0.990 ± 0.001
	0.1		$8.16 \pm 0.67 \cdot 10^{-4}$	0.997	0.997 ± 0.001
α-Fe_2O_3/quartz/ΔQ (this study)	0.001	0.51	$8.98 \pm 0.37 \cdot 10^{-4}$	0.928	0.930 ± 0.001
		0.98	$1.34 \pm 0.05 \cdot 10^{-3}$	0.948	0.949 ± 0.001
		1.9	$2.60 \pm 0.13 \cdot 10^{-3}$	0.941	0.941 ± 0.001
		3.2	$4.61 \pm 0.34 \cdot 10^{-3}$	0.939	0.940 ± 0.001
		7.3	$8.60 \pm 0.22 \cdot 10^{-3}$	0.947	0.948 ± 0.001
		11.7	$1.12 \pm 0.14 \cdot 10^{-2}$	0.936	0.944 ± 0.001
		11.7	$1.24 \pm 0.12 \cdot 10^{-2}$	0.941	0.939 ± 0.001
$Cr(OH)_3$/glass/ΔI (45)	0.0032	0.75–1.0	$6.53 \pm 0.16 \cdot 10^{-4}$		0.133 ± 0.006
	0.023		$5.89 \pm 0.16 \cdot 10^{-4}$		0.345 ± 0.004
	0.043		$5.68 \pm 0.69 \cdot 10^{-4}$		0.627 ± 0.015
	0.10		$4.12 \pm 0.42 \cdot 10^{-4}$		0.754 ± 0.011
	0.20		$3.57 \pm 1.12 \cdot 10^{-4}$		0.899 ± 0.016

[a] Fitted rate coefficeint (k_{fit}), fraction remaining (C_{eq}), and standard errors determined by fitting data according to Eq. [2].

constant (J) for solids 1 and 2 in medium 3. The Hamaker constant depends on the atomic density and polarizability of the solids and medium; it may be estimated from theory or determined by experiment. For oxides in aqueous suspension, A_{132} ranges from about 0.3×10^{-20} to 5×10^{-20} J (14, 29). We used $A_{132} = 1 \times 10^{-20}$ J for the quartz:water:hematite system because quartz:water:quartz interaction is characterized by $A_{132} = 0.8 \times 10^{-20}$ J and the self-interacting Hamaker constants of metal oxides are slightly greater than that of quartz (14).

Short-range repulsive forces dominate $\phi^{tot}(x)$ at very short separation distances; thus, they may have an extremely important effect on colloid detachment (13, 15, 18). However, neither the spatial variation nor the origins of the short-range repulsion are well understood. Short-range repulsive forces have been attributed to solvation forces that arise from the structuring of liquid molecules confined between two surfaces (30). The short-range repulsion has often been calculated as the Born potential energy, which is derived from the repulsive term of the interatomic Lennard–Jones m–n potential. The Born potential has been formulated for sphere–sphere interaction with an x^{-12} dependence on distance (31),

$$\phi^{Born} = \frac{A}{75600r}\left(\frac{\sigma}{a_c}\right)^6 \times \left[\frac{-4r^2 - 14(y-1)r - 6(y^2-7y+1)}{(2r-1+y)^7} + \frac{-4r^2 + 14(y-1)r - 6(y^2-7y+1)}{(2r+1-y)^7} + \frac{4r^2 + 14(y-1)r + 6(y^2+7y+1)}{(2r+1+y)^7} + \frac{4r^2 - 14(y-)r + 6(y^2+7y+1)}{(2r-1-y)^7}\right], \quad [5]$$

where σ is the collision parameter (m). For interatomic interactions, σ has been determined experimentally to be on the order of 5 Å (31). Initially, we used $\sigma = 5$ Å, but because we felt that this short-range repulsion was the least understood of the three potentials, we used σ as a fitting parameter to force the calculated potential energy profiles to agree with the experimental data. As a result, our fitted Born collision parameter may actually reflect various near-surface repulsive forces including hydration and steric effects.

Hogg *et al.* (32) calculated the double layer potential using a linearized approximation of the Poisson–Boltzmann equation adapted to sphere–sphere interaction by one-dimensional integration of plate–plate interaction for the constant potential case,

$$\phi^{dl} = \frac{\pi\epsilon\epsilon_0 a_c a_g}{a_c + a_g}\left\{2\psi_{0c}\psi_{0g}\ln\left[\frac{1+e^{-\kappa x}}{1-e^{-\kappa x}}\right] + (\psi_{0c}^2 + \psi_{0c}^2)\ln[1-e^{-2\kappa x}]\right\}, \quad [6]$$

where ϵ is the dielectric constant of water (dimensionless), ϵ_0 is the permittivity of free space (C V^{-1} m^{-1}), and ψ_{oi} is the surface potential of the colloid or collector grain. The reciprocal double layer thickness κ (m^{-1}) is expressed as

$$\kappa^2 = \frac{2000 N_a I e^2 z^2}{\epsilon\epsilon_0 kT}, \qquad [7]$$

where N_a is Avogadro's number, I is ionic strength (mole $liter^{-1}$), e is the elementary charge (C), z is the valence of a symmetrical electrolyte, k is the Boltzmann constant (J K^{-1}), and T is the absolute temperature. Hogg *et al.* (32) showed that the plate–plate form of this expression was reasonably accurate (compared to an exact solution) for $\psi <$ 100 mV and $\kappa a_c > 10$. Although the hematite and quartz surfaces were characterized by ψ values as large as −250 mV, we used Eq. [6] because of the ease of its calculation. The constant potential case describes a double layer in which equilibrium with ions in the bulk solution is maintained with respect to the time scale of colloid attachment and detachment (33, 34). The constant potential case seems to be appropriate for the colloid detachment because the intersurface domain seems to rapidly equilibrate with changes in bulk solution chemistry.

Surface potentials. It is generally recognized that ζ-potentials are not good estimates of ψ_0, especially under conditions of high surface charge and high I (13, 35–38). Therefore, we used a surface complexation/double layer (SCDL) model to estimate surface potentials (ψ_{scdl}). Surface potentials were determined for an interface modeled by a set of proton exchange reactions in the presence of a diffuse (Gouy–Chapman) double layer populated by indifferent counterions. Surface complexation equilibrium was solved with a version of MINEQL (39) adapted to account for the diffuse double layer interactions (38). Parameters used to calculate ψ_{scdl} included the total active site density $[>M\text{–OH}]_{tot}$, the intrinsic acidity constants pK_{a1}^{int} and pK_{a2}^{int}, the specific surface area S_s, and suspension concentration χ_s of the oxide (Table 2). Oxide site densities vary considerably with measurement technique (41); therefore, we assumed a site density of 4 sites nm^{-2} for the oxides in these experiments. The intrinsic acidity constants were estimated by centering ΔpK^{int}, the difference between values of pK_{a1}^{int} and pK_{a2}^{int}, on the point of zero charge (pH_{zpc}) determined by microelectrophoresis. The calculated values of ψ_{scdl} are substantially greater than ζ potentials typically measured for these oxides (Table 3).

Calculation of detachment energies. Colloid release from grain surfaces is a two-step mechanism consisting of (1) detachment from the surface and (2) diffusion from the surface to the advecting bulk fluid (Fig. 1). The rate of the first step, colloid detachment, depends on the size of the intersurface potential energy barrier (16–18). In the diffusion boundary layer near the grain surface, where fluid motion is negligible relative to colloid diffusion, colloid attachment and detachment have been described as a first-order exchange between colloids in the primary minimum (C_{min1}) and colloids in the bulk fluid (C_{fl}),

$$C_{min1} \underset{k_{att}}{\overset{k_{det}}{\rightleftharpoons}} C_{fl}, \qquad [8]$$

where k_{det} and k_{att} (s^{-1}) are the detachment and attachment rate coefficients. We assume that $[C_{min1}]$, the concentration of colloids in the primary minimum (g m^{-3}, where the volume (m^3) is defined as the product of the grain surface area (m^2) and one colloid diameter (m) for up to monolayer coverage), may be equated with $[C_s]$, the experimentally determined concentration of attached colloids (g m^{-3}). This scheme assumes that all attachment sites are characterized by the same potential energy, but this is clearly a simplification. $[C_{fl}]$ is the colloid concentration in the bulk fluid (g m^{-3}). In an analogy with Arrhenius kinetics, the rate coefficients have been exponentially related to the size of the activation energy barriers (18),

$$k_{det} \approx D_c(x_{max}) \frac{(\gamma_{max}\gamma_{min1})^{1/2}}{2\pi kT} \times \exp\left(-\frac{(\phi_{max} - \phi_{min1})}{kT}\right) \qquad [9a]$$

TABLE 2
Parameters Used in the Calculation of Surface Potentials with a Surface Complexation/Double Layer Model

Colloid or grain	Mean diameter (μm)	pH_{zpc}	ΔpK^{int}	S_s (m^2 g^{-1})	χ_s (g L^{-1})	(Ref.)
α-Fe_2O_3	0.15	8.0	3.0	75	2.6	(this study)
Quartz	250	2.5	9.0	0.1	1500	(this study)
$Cr(OH)_3$	0.28	8.2	3.0	75	0.88	(45)
Glass	53	2.5	9.0	0.2	1800	(45)

Note. The parameters were measured or estimated by the following techniques: Mean diameter: SEM, PCS, sieving. pH_{zpc}: microelectrophoresis; quartz (40). ΔpK^{int}: acid–base titration; iron oxide (41), quartz and glass (42). S_s: estimated from BET specific surfaces area (41) and suppliers' data. χ_c: estimated from colloid and grain size, number concentration, specific density, and column volume and porosity data.

TABLE 3

Summary of Solution Composition, Surface Potential, and Detachment Energies Estimated for σ = 20 Å for Colloid Detachment in the Hematite–Quartz System of This Study and in the Model Systems of Kolakowski and Matijević (45)

Colloid/grain/exp. (ref.)	pH	$NaNO_3$ (M)	I (M)	Colloid ζ mV	Colloid ψ_{scdl} mV	Grain ζ mV	Grain ψ_{scdl} mV	ϕ^{det} (/1000kT)
α-Fe_2O_3/quartz/ΔI	7.0	1.0×10^{-3}	1.0×10^{-3}	—	+54.7	—	−99.0	−2.37
(this study)	11.0		1.0×10^{-3}	—	−154	—	−248	3.36
	11.0	2.0×10^{-3}	3.0×10^{-3}	—	−146	—	−235	3.04
	11.0	9.0×10^{-3}	1.0×10^{-2}	—	−136	—	−217	2.55
	11.0	2.9×10^{-2}	3.0×10^{-2}	—	−127	—	−199	2.01
	11.0	9.9×10^{-2}	1.0×10^{-1}	—	−116	—	−174	1.30
$Cr(OH)_3$/glass/ΔI								
(45)	7.2		3.2×10^{-3}	—	+46.9	—	−78.8	−2.27[a]
	11.5		3.2×10^{-3}	−47.0	−159	−137	−221	6.25
	11.5	2.0×10^{-2}	2.3×10^{-2}	—	−142	—	−197	4.38
	11.5	4.0×10^{-2}	4.3×10^{-2}	—	−137	—	−187	3.69
	11.5	1.0×10^{-1}	1.0×10^{-1}	—	−128	—	−172	2.65
	11.5	2.0×10^{-1}	2.0×10^{-1}	—	−121	—	−159	1.85

[a] Data not collected at pH 7.2. It has been assumed that no colloid release would have occurred at pH 7.2, the pH_{zpc} of the $Cr(OH)_3$ colloid, in order to determine x_{min1} in the same manner as for the α-Fe_2O_3 colloids.

$$k_{att} \approx D_c(x_{max})\left(\frac{\gamma_{max}}{2\pi kT}\right)^{1/2} \exp\left(-\frac{\phi_{max}}{kT}\right), \qquad [9b]$$

where $D_c(x_{max})$ is the colloid diffusion coefficient ($m^2\ s^{-1}$) at the separation distance x_{max} of the primary maximum (ϕ_{max}), and

$$\gamma_i = -\left.\frac{d^2\phi_i}{dx^2}\right|_{x_i}, \qquad [10]$$

where ϕ_i is the potential energy at the primary minimum (ϕ_{min1}) or ϕ_{max}, and x_i is the separation distance of ϕ_{min1} or ϕ_{max}. When $[C_{fl}]$ is maintained at low concentrations by advection of colloid-free fluid, the attachment rate is negligible and the observed colloid release rate (k_{exp}, s^{-1}) may be approximated as

$$\frac{d[C_{fl}]}{dt} = k_{exp}[C_s] \simeq k_{det}[C_{min1}] \qquad [11]$$

for detachment-limited release (Fig. 1, Case B). Thus, the rate is expected to be exponentially related to the size of the energy barrier opposing detachment, $\phi^{det} = -(\phi_{max} - \phi_{min1})$. Values of ϕ_{max} and ϕ_{min1} were identified from ϕ^{tot} profiles calculated with separation distance resolutions of $\Delta x = 2 \times 10^{-11}$ m in the vicinity of ϕ_{min1} and ϕ_{max}.

For the case in which the energy barrier no longer exists in the potential energy profile (Fig. 1, Case C), the rate of colloid release to the bulk fluid is limited by the diffusion of colloids across the hydrodynamic boundary layer. The hydrodynamic boundary layer is the fluid adjacent to the surface in which colloid diffusive transport dominates over advective transport. In this case,

$$\frac{d[C_{fl}]}{dt} = k_{exp}[C_s] \simeq k_{dif}[C_{det}], \qquad [12]$$

where k_{dif} (s^{-1}) is the rate coefficient associated with colloid diffusion across the boundary layer.

RESULTS

In the hematite–quartz system, a maximum of about 7% of the colloids were removed by the pH 11.0 solutions. SEM/EDX examination of the quartz surfaces showed that the remaining hematite colloids were primarily situated in rough, weathered areas (Fig. 2). Quantification of the Fe peak areas observed on 10 quartz grains revealed that the weathered areas contained 4.1 ± 1.4 mole% Fe ($\pm 1\sigma$) and that the smooth areas contained 1.4 ± 0.7 mole% Fe. Individual colloids could not be resolved by SEM, probably because the poorly conducting quartz was insufficiently coated with Au–Pd.

The size of hematite colloids in the column eluent, as measured by PCS, never varied by more than ±10% from the size of the colloids attached to the quartz grains, indicating that single colloids were detached from quartz surfaces and that the dilute colloid suspensions generated by detachment did not coagulate rapidly even at I = 0.1 M.

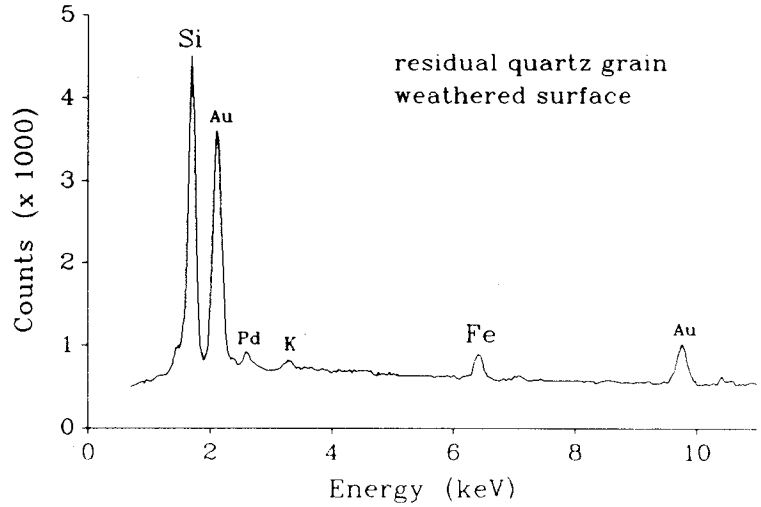

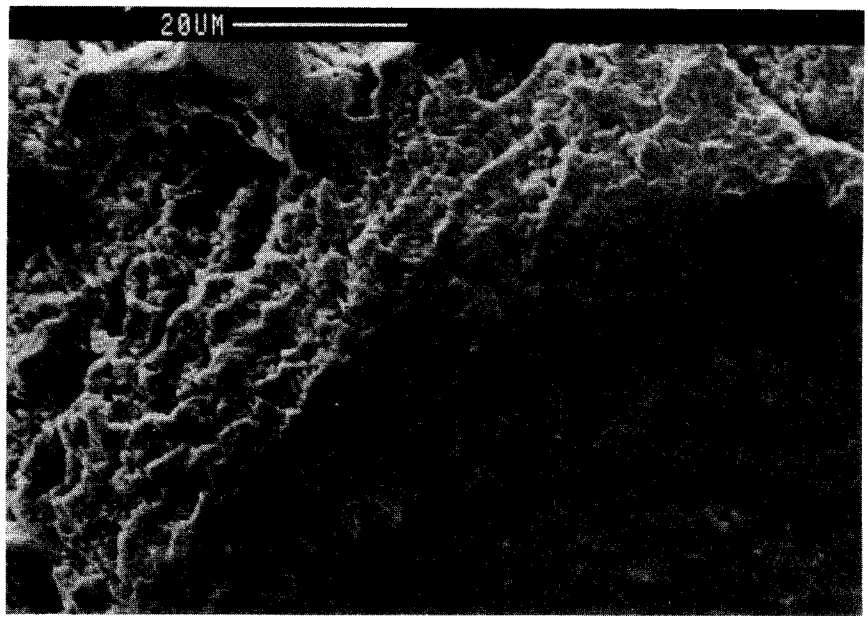

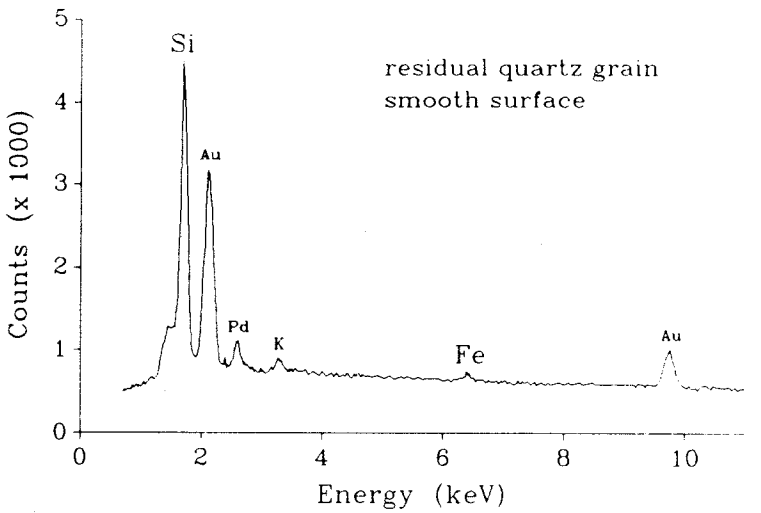

FIG. 2. SEM photograph of a quartz grain following the removal of 7.2% of the originally attached colloids by 100 pore volumes of pH 11.0, $I = 1 \times 10^{-3}$ M flush solution at 0.51 ml min^{-1}. EDX spectra measured over ~4 μm^2 areas show that hematite colloids were more abundant on the weathered, irregular surface than on the smooth surface. Similar results were observed on other quartz grains.

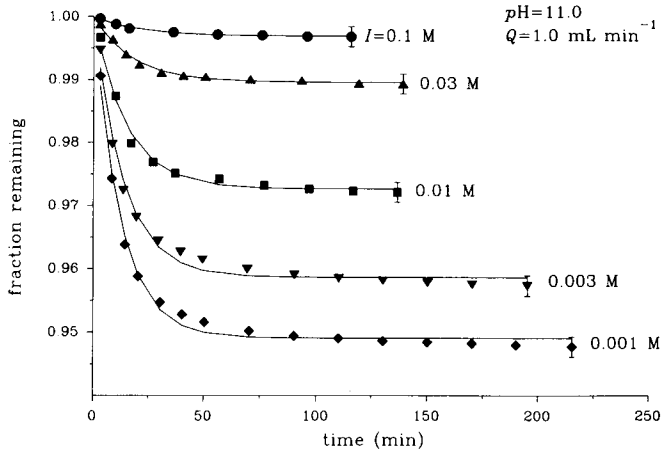

FIG. 3. Plot of the fraction of hematite colloids remaining attached to quartz grains vs time for pH 11.0 flushing solutions of varying ionic strength (initial conditions are pH 7.0, I 0.001 M). Both the release rate and the total fraction released increased with decreasing ionic strength. Lines show best fit of Eq. [2] to data. Error bars on final points show detection limits.

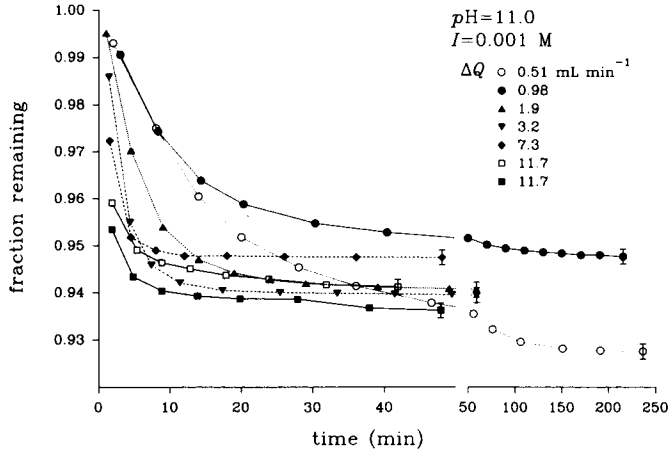

FIG. 5. Plot of the fraction of hematite colloids remaining attached to quartz grains vs time as flow rate was varied from 0.51 to 11.7 ml min^{-1}. Release rates increased with increasing flow rate, but the total fraction of colloids removed did not vary significantly with flow rate. Error bars show detection limit.

The increase in I had two effects on colloid detachment (Fig. 3): (1) a decrease in the initial detachment rate and (2) a decrease in the fraction of colloids ultimately released. We calculated (using σ = 5 Å) that the increase in I produced a decrease in the size of the energy barrier until the energy barrier actually vanished for the I = 0.1 M case (Fig. 4); thus, the release rates *were not inversely related* to the size of the energy barriers, as this colloid detachment model predicts.

Increasing the flow rate resulted in an increase in the detachment rate (Fig. 5), but the fraction of colloids ultimately released did not vary significantly with flow rate. The range of the observed fractions remaining, 0.928 to 0.948, was within 2σ of the mean observed fraction remaining, 0.940 ± 0.006. The observed fractions remaining closely matched those determined by fitting the ΔQ data by first-order exponential decay (C_{eq}, Table 1), indicating that the experiments had been run to equilibrium. If the colloid release rates are normalized to the number of pore volumes passing through the column instead of to time, it is evident that the effect of flow rate on observed colloid release is not simply a function of pore fluid residence time (Table 4).

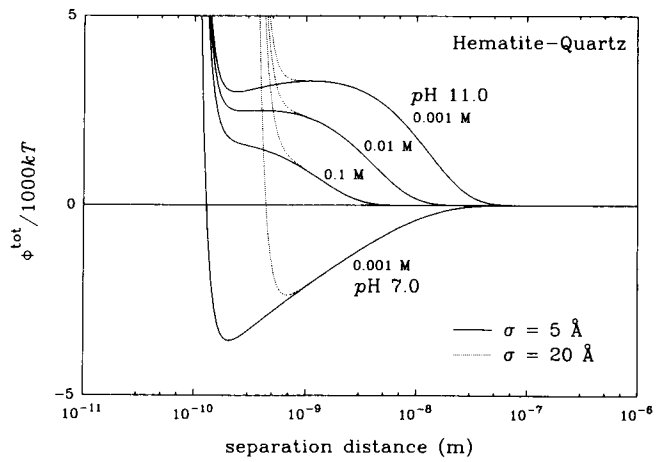

FIG. 4. Plot of total potential energy (ϕ^{tot}) vs separation distance for the hematite–quartz system. An increase in the Born collision parameter σ from 5 to 20 Å caused the energy barriers to vanish.

DISCUSSION

Release Rate–Energy Barrier Relationship

For the hematite–quartz system at pH 11, our data indicate that the rate-limiting step in colloid release was not colloid

TABLE 4
Rate Coefficients Normalized to the Number of Pore Volumes Passing through the Column for the ΔQ Experiments

Flow rate Q (mL min^{-1})	Pore volume V_{pore} (mL)	Residence time (min)	Fitted[a] rate coefficient k_{fit} (mL^{-1})	Fitted[a] fraction remaining C_{eq}
0.51	1.69	3.31	0.178 ± 0.007	0.930 ± 0.001
0.98	1.79	1.83	0.166 ± 0.010	0.949 ± 0.001
1.9	1.69	0.89	0.139 ± 0.007	0.941 ± 0.001
3.2	1.54	0.48	0.133 ± 0.010	0.940 ± 0.001
7.3	1.69	0.23	0.120 ± 0.003	0.948 ± 0.001
11.7	1.64	0.14	0.095 ± 0.012	0.944 ± 0.001
11.7	1.54	0.13	0.098 ± 0.009	0.940 ± 0.001

[a] Fitted rate coefficient (k_{fit}), fraction remaining (C_{eq}), and standard errors determined by fitting data from plots of fraction remaining vs number of pore volumes according to a form of Eq. [2] with the number of pore volumes substituted for time.

transport "over an energy barrier." We did not observe any correlation between the release rate coefficients and the size of the energy barriers. Also, the release rate depended on the flow rate. An alternative explanation for these results is that the energy barrier was absent from the potential energy profile when hematite colloid release was observed at pH 11.

We surmise that the calculated potential energy profiles did not accurately represent the intersurface interactions. It is likely that the potential energies that we calculated for very small separation distances (where the primary minimum is located) are not accurate. The double layer and London–van der Waals forces have been validated down to separation distances of about 10 molecular layers of water, or about 4 nm, but interactions at smaller separation distances do not agree with calculated forces owing to a variety of effects (30). When surfaces are separated by less than about 10 water molecules, it is no longer possible to treat the water as a structureless continuum. Between hydrophilic surfaces, repulsive hydration forces begin to oscillate at smaller separation distances owing to molecular size and shape and local bonding of water (43).

Although the Born potential was derived from the same interatomic potential from which the London–van der Waals potential was derived, it clearly does not accurately represent the complicated interactions between surfaces at small separation distances. This should not be surprising, because two parameters in the Born potential expression have been determined for interatomic systems. According to Feke *et al.* (31), a value of $n = 12$ has typically been used for the dependence of the Born potential on separation distance, x^{-n}, and the value of the collision parameter, σ, has been determined experimentally to be on the order of 5 Å. These values have been applied to colloidal systems without justification of their transferability.

Owing to the lack of agreement between the colloid release data and intersurface potential energy, we varied σ as a "fitting parameter" until we found a value of σ that produced potential energy profiles without energy barriers for the conditions under which colloid release was observed. When we increased σ from 5 to 20 Å, we found that ϕ_{min1} and ϕ_{max} disappeared for the pH 11.0 experiments; that is, the energy barrier to detachment no longer existed regardless of which ionic strength was involved (Fig. 4). For the pH 7.0 experiment, in which colloid release was not observed, the energy barrier remained, even with $\sigma = 20$ Å. The disappearance of the energy barrier from the potential energy profile implies that repulsive forces prevailed at all separation distances.

If such intersurface energy profiles are appropriate, we would argue that colloid detachment was actually aided by intersurface forces during the pH 11.0 experiments and limited only by diffusion from the surface to the bulk fluid. For the pH 11.0 potential energy profiles from which the energy barriers disappeared, we quantified ϕ^{det} as the potential energy at the separation distance where ϕ_{min1} existed for the pH 7.0 case with $\sigma = 20$ Å ($x_{min1} = 7.0$ Å). The colloid release rate coefficients correlated well with these detachment activation energies (Fig. 6), suggesting that the detaching colloids received a repulsive "push" corresponding to the magnitude of the potential energy at the separation distance at which they had been attached.

The increase in σ from 5 to 20 Å results in an increase in the effective "distance of closest approach," or x_{min1}, from 2.0 to 7.0 Å for the pH 7.0 case. This effective distance of closest approach may be thought of as the separation distance where the short-range repulsive potential, whatever its origin, begins to dominate the potential energy profile. Distances of closest approach ranging from 4 to 10 Å have been determined from results of other colloid release experiments (27, 44–47). These distances of closest approach represent the application of a "hard-sphere" potential as an alternative to the "soft" Born potential (48). Both repulsive potentials are employed to remove the infinitely deep primary minimum (from which the probability of attached colloids escaping is zero) predicted when only London–van der Waals and double layer potentials are used. The disappearance of energy barriers in our system could have been characterized equally well by shifting a hard-sphere potential from 2.0 to 7.0 Å.

Effect of Fluid Velocity on Detachment Rate

When ionic strength was decreased by two orders of magnitude, k_{exp} increased by only 64%. In contrast, an increase in the flow rate by a factor of 22.9 caused k_{exp} to increase by a factor of 13.8. Note that the increase in release rate with flow was not simply related to a change in column residence time; if colloid release rate coefficients are normalized to dimensionless time (number of pore volumes), the release rate coefficients decrease with increasing flow rate (Table 4).

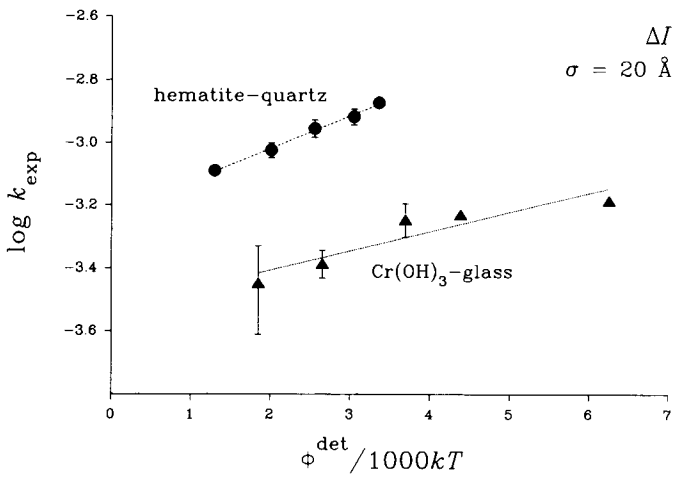

FIG. 6. Logarithmic plot of experimental rate coefficients (k_{exp}) vs detachment energies ($\phi^{det}/1000kT$) for $\sigma = 20$ Å in the hematite–quartz and $Cr(OH)_3$–glass ΔI experiments.

The sensitivity of the release rate to the flow rate indicated that, in these experiments, the rate-limiting step in colloid release was not detachment from the primary minimum; instead, the rate-limiting step was dominated by hydrodynamics. In experiments of latex colloid release from sand, McDowell-Boyer (49) also observed that the rate of colloid mobilization depended on flow rate at relatively low flow rates.

We postulate that the rate-limiting step in colloid release in the hematite–quartz system at pH 11 was diffusion of detached colloids across the boundary layer between grain surfaces and the bulk fluid (Fig. 1, Case C). The role of hydrodynamic parameters in colloid release can be described by designating C_{det} as the concentration of detached colloids at the edge of the region over which the intersurface potential extended (δ_ϕ);

$$C_{min1} \underset{k_{att}}{\overset{k_{det}}{\rightleftharpoons}} C_{det} \xrightarrow{k_{dif}} C_{fl}, \qquad [13]$$

where k_{dif} is a first-order rate coefficient (s^{-1}) reflecting diffusive transport of detached colloids across the diffusion boundary layer. If advection maintains $[C_{fl}]$ at low levels, diffusion-driven transport from the bulk fluid to the surface can be neglected and the rate of colloid removal from C_{det} may be expressed as

$$\frac{d[C_{det}]}{dt} = -D_c \frac{d^2[C_i]}{dx^2}\bigg|_{C_{det}}^{C_{fl}}$$

$$= -\frac{D_c}{\delta_{bl}^2}[C_{det}]. \qquad [14]$$

Thus, k_{dif} (and k_{exp}, approximately) depend on the colloid diffusion coefficient and the boundary layer thickness for diffusion-limited release (Fig. 1):

$$k_{exp} \simeq k_{dif} = \frac{D_c}{\delta_{bl}^2}. \qquad [15]$$

D_c is given by the Stokes–Einstein equation,

$$D_c = \frac{kT}{6\pi\mu_{fl}a_c}, \qquad [16]$$

where μ_{fl} is the viscosity of the fluid ($kg\ m^{-1}\ s^{-1}$). The average thickness of the boundary layer around a single spherical colloid in laminar flow may be estimated by (50)

$$\delta_{bl} \sim a_g\left(\frac{D_c}{Ua_g}\right)^{1/3}, \qquad [17]$$

where U ($m\ s^{-1}$) is the pore velocity of the bulk fluid, defined as $Q_{col}/(A_{col}n)$, where A_{col} is the cross-sectional area of the column (m^2), and n is the porosity of the packed column (void volume/total volume).

Combining these expressions, we expect that for diffusion-limited release

$$k_{exp} \simeq \left(\frac{kT}{6\pi\mu_{fl}a_c}\right)^{1/3} a_g^{3/4} U^{2/3} \qquad [18]$$

and, for the conditions of our experiment,

$$k_{exp} \simeq 10^{1.36}U^{0.67}. \qquad [19]$$

Linear regression of a logarithmic plot (see Fig. 7) of k_{exp} vs. U results in

$$k_{exp} = 10^{1.01\pm0.10}U^{0.84\pm0.02}. \qquad [20]$$

This fitted relationship appears to be reasonably close to the theoretical prediction.

Alternatively, it is possible that the colloid release rate may have been affected by hydrodynamic shear, although it is likely that colloid removal by shear would have resulted in an increase in the total fraction of colloids released and this did not occur. Researchers studying the release of submicrometer colloids from grains under laminar flow have concluded that hydrodynamic shear forces are negligible compared to electrostatic adhesive forces (11, 45, 51, 52). For larger colloids and more rapid flows, colloid release has been attributed to colloid rolling initiated by fluid drag force tangential to the surface (53, 54). The effect of hydrodynamic lift forces on detachment is considered negligible compared to the effect of the tangential force (49, 55). An analysis of the tangential and adhesion forces for these experiments showed that the force of adhesion for colloids in the primary

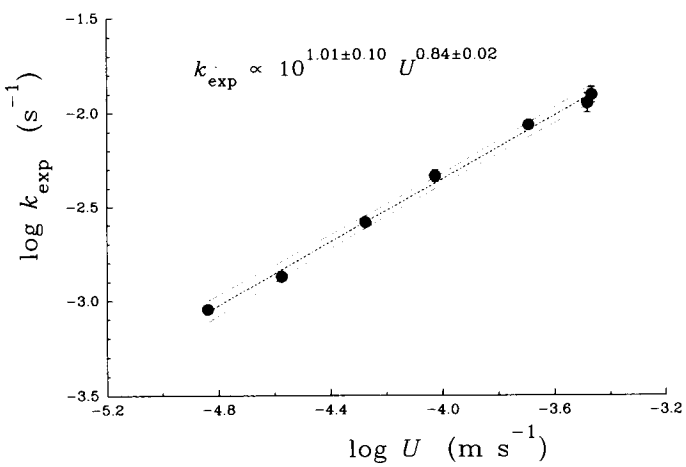

FIG. 7. Logarithmic plot of rate coefficients (k_{exp}) vs the bulk fluid flow velocity U. The dependence of k_{exp} on U shown in Eq. [20] is reasonably close to the theoretically predicted relationship shown in Eq. [19].

minimum at pH 7 was five orders of magnitude greater than the tangential force at the highest flow rate (26).

Fraction of Colloids Released

After 10 to 100 pore volumes of flushing in the ΔI experiments, colloid concentrations in the eluent dropped to near-zero levels after a relatively small fraction of the colloids were released. The total fraction of colloids released at the final sample time decreased with increasing ionic strength (Fig. 3). We surmise that lower ionic strengths caused increasing repulsion that led to the more effective release of colloids attached to the surface. The decrease in the fraction of colloids released with each increase in I suggests that colloid attachment is characterized by a distribution of attachment energies, as proposed by Kallay *et al.* (23). The distribution of attachment energies may be attributed to irregular geometries associated with cracks and crevices on the grain surfaces. The SEM/EDX analysis suggested that Fe was concentrated on the weathered portions of the quartz surfaces (Fig. 2). The implications of this observation would be that the majority of the hematite colloids remained attached to the quartz surfaces because the change in solution conditions did not cause enough repulsion to remove them. The removal of these colloids by sonication at the conclusion of the experiments indicated that chemical bonding was not involved, in agreement with the conclusions of Kolakowski and Matijević (45).

Alternatively, some fraction of the colloids may have been detached from the primary minimum upon pH change and then reattached following lateral diffusion to sites of higher attachment energy. Kuo and Matijević (47) observed that hematite colloids were transferred from smooth to crenelated surfaces on steel grains during flushing and that a maximum of only 12% of the colloids were removed from these steel grains. The colloids appeared to have aggregated into larger flocs in their experiment, which would further inhibit their detachment owing to a decrease in the diffusion coefficient. Lateral diffusion to higher energy sites would have to occur without transport to the bulk fluid because reattachment of colloids that reach the bulk fluid is unlikely. The return of colloids to the surface from the bulk fluid would be opposed by a large attachment energy barrier and the diffusion gradient. Indeed, colloid suspensions readily passed through columns without attaching at the high pH values that promoted detachment (46, 47).

Review of Related Colloid Detachment Data

The dependence of colloid detachment kinetics on ionic strength was measured in a series of model systems by Matijević and co-workers (α-Fe_2O_3–glass, 27; $Cr(OH)_3$–glass, 45; and β-FeOOH–steel, 56); however, we were able to compare our results to those of Kolakowski and Matijević (45) only. In the α-Fe_2O_3–glass system, Kallay *et al.* (27) observed an *increase in colloid release rate with increasing ionic strength,* a result at odds with those observed in our hematite–quartz system, the $Cr(OH)_3$–glass and β-FeOOH–steel systems, and field and laboratory observations (10, 11, 49, 52). This counterintuitive result was attributed to the use of a shorter column that supposedly reduced the probability of reattachment of released colloids that would normally be promoted at high I (23). When we estimated the probability of reattachment based on the frequency of colloid collisions with grains and the surface area of grains along the flow path (26), we found that reattachment probability in the α-Fe_2O_3–glass system (27) was actually two to three times higher than that in the $Cr(OH)_3$–glass (45) and β-FeOOH–steel (56) systems and approximately the same as in our hematite–quartz system. Furthermore, Kuo and Matijević (46) concluded that colloid reattachment was negligible after showing that Fe_2O_3 colloids passed through a column of clean steel grains at pH $\geq$ 9 without attachment. Owing to the lack of explanation for the counterintuitive results obtained by Kallay *et al.* (27), we have not considered their results further here. We also did not consider the β-FeOOH–steel system (56) because (1) the colloids were not spherical and (2) plots of the fraction remaining vs time were not provided.

For the $Cr(OH)_3$–glass (45) system, we estimated experimental rate coefficients by fitting the reported colloid release data with Eq. [2]. Originally, the rate coefficient estimated for the lowest value of I (0.0032 M) was less than that of the next higher value of I (0.023 M) because the first data points on the fraction remaining vs time curves coincided. However, 89% of the colloids were ultimately removed at I = 0.0032 M and only 64% were removed at I = 0.023 M, suggesting that the first data points for these values of I may have coincided owing to experimental error. When the first points were removed from the two data sets, more appropriate rate coefficients were estimated and used in the analysis (Table 1). The small variation in the rate coefficients over nearly two orders of magnitude variation in I is similar to that observed for our hematite–glass system.

Kolakowski and Matijević (45) measured ζ only at the lowest value of I tested in ΔI experiment, so we estimated ψ_{scdl} for the oxides using the parameters listed in Table 2. For $Cr(OH)_3$, we used the same ΔpK^{int} and S_s as for the Fe oxides. Potential energy profiles were calculated using σ = 5 and 20 Å. With σ = 5 Å, a substantial energy barrier is predicted to exist at low I, but with σ = 20 Å, the energy barrier is predicted to be absent as for the hematite–quartz system (Fig. 8). For σ = 20 Å, detachment energies were estimated by (1) calculating values of ψ_{scdl} for the colloid and grain at pH 7.2 (one pH unit below the pH_{zpc} of $Cr(OH)_3$) to simulate conditions under which colloids would not be released, (2) calculating a potential energy profile for pH 7.2, (3) determining x_{min1} for pH 7.2, and (4) using $\phi^{tot}(x_{min1})$ as ϕ^{det} for the pH 11.5 runs during which colloid release was observed. The separation distance at which the

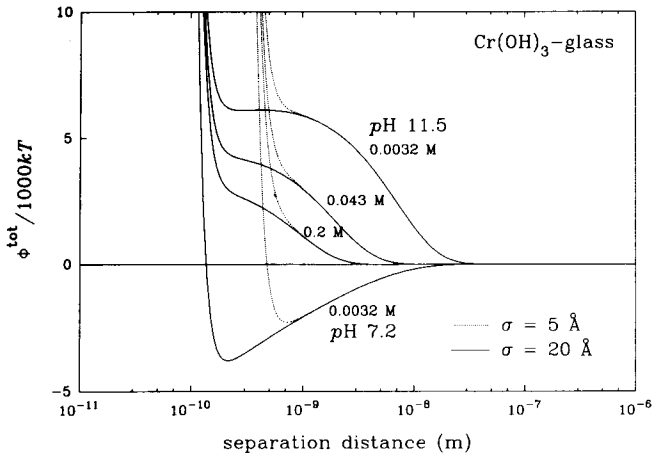

FIG. 8. Plot of total potential energy vs separation distance for the $Cr(OH)_3$–glass system. The energy barrier still exists at the lowest value of I for σ = 5 Å, but energy barriers have vanished at σ = 20 Å.

detachment energy was calculated was x_{min1} = 7.0 Å, the same value used for our hematite–quartz system. The colloid release rate coefficients correlated well with the detachment energies for the $Cr(OH)_3$–glass system (Fig. 5), but the slope and intercept of the log k_{exp} vs. ϕ^{det} relationship determined for hematite–quartz ($m = 2.5 \pm 0.1 \times 10^{16}$ J^{-1}, $b = -3.2 \pm 0.1$) were significantly different from those determined for $Cr(OH)_3$–glass ($m = 1.5 \pm 0.4 \times 10^{16}$ J^{-1}, $b = -3.5 \pm 0.1$).

Although the $Cr(OH)_3$–glass and hematite–quartz systems possessed quite similar surface potentials at given ionic strengths, the detachment energies calculated for the $Cr(OH)_3$–glass system were about 1.5 to 2 times greater than those calculated for the hematite–quartz system. The repulsive double layer potentials and, hence, the detachment energies for $Cr(OH)_3$–glass were greater because the $Cr(OH)_3$ colloids were about twice as large as the hematite colloids. Nevertheless, the $Cr(OH)_3$ colloids were released about half as rapidly as the hematite colloids. This may suggest that colloid release was limited by diffusion across the boundary layer in the $Cr(OH)_3$–glass system. The diffusion coefficient of the $Cr(OH)_3$ colloids is about one-half that of the hematite colloids and the release rate coefficient in a diffusion-limited case is directly related to the diffusion coefficient; thus, the slower release of $Cr(OH)_3$ colloids is consistent with diffusion-limited release.

Implications for Colloid Release

In experiments exploring the effects of changes in solution chemistry on the rate of colloid release, Fogler and co-workers (11, 57, 58) reported that colloid release occurred suddenly when ionic strength or $[H^+]$ reached a threshold beyond which colloids were mobilized. In these and other experiments (49, 52), colloid release occurred under conditions for which DLVO calculations predicted that detachment energy barriers were still present. With energy barriers still present, the rates of colloid release predicted by the energy barrier model would be much lower than the measured rates of colloid release reported in these studies, much as predicted deposition rates are vastly different from measured deposition rates.

We hypothesize that the threshold values responsible for rapid colloid mobilization actually correspond to the conditions at which the detachment energy barriers disappear and the rates of colloid release are no longer limited by detachment from the surface. McDowell-Boyer (49) observed that colloid release depended on flow rate, substantiating this supposition. Khilar and Fogler (11) and Cerda (52) claimed that variations in flow rate did not affect colloid release rates; however, they quantified drops in the hydraulic conductivity of the columns and not the actual rates of colloid release. Because these researchers calculated double layer potentials using ζ potentials, it is likely that the repulsive interactions were substantially underestimated. It has long been recognized that ζ potentials do not accurately represent surface potentials.

It should be noted that the double layer potential calculated by the linear approximation of the Poisson–Boltzmann equation formulated by Hogg *et al.* (32) is greater than that calculated by the nonlinear, or exact, solution provided by Overbeek (59) at most separation distances. However, comparison of the linear and nonlinear solutions with direct measurements of the force between cleaved mica surfaces (60) showed that, while the Overbeek solution closely matched the experimental results, the linear approximation actually underestimated the measured double layer potential at separation distances less than about 10 nm (61). Thus, the repulsive interactions between the hematite–quartz and $Cr(OH)_3$–glass surfaces may have been underestimated at the separation distances in the vicinity of the primary minimum and maximum by the Hogg *et al.* expression. If this is true, it may have been that using calculated surface potentials instead of ζ potentials would have been sufficient to produce the potential energy profiles without detachment energy barriers that best describe the colloid release data.

CONCLUSIONS

In the energy barrier model of colloid release kinetics, colloid release is limited by the rate of diffusion of colloids over an intersurface potential energy barrier opposing detachment (16–18). The detachment rate coefficients are thought to be inversely related to the size of the energy barrier in an Arrhenius-type relationship. However, in a system of hematite colloids and quartz grains, both observed colloid release rates and the size of the energy barriers decreased as

ionic strength was increased. The colloid release rates also increased with increases in the flow rate. These experimental results indicated that the colloid transport over the detachment energy barrier was not the rate-limiting step in colloid release.

To explain these data, we suggest that the change in solution chemistry caused the energy barriers to disappear from the potential energy profile. Under such circumstances, repulsive forces would exist at all separation distances and attached colloids would be "pushed" away from the surface. Then, the rate-limiting step in colloid release would be the transport of detached colloids to the bulk fluid.

Using the collision parameter σ in the Born short-range repulsion expression as a fitting function, we produced potential energy profiles without detachment energy barriers for the experimental conditions under which colloid release was observed by increasing σ from 5 to 20 Å. This increase in σ resulted in an increase in the effective distance of closest approach from 2.0 to 7.0 Å, a value that agrees well with distances of closest approach determined by others (25, 44–47). The effect of the variation in flow rate on the colloid release rate was reasonably consistent with the theoretical prediction based on colloid diffusion coefficients and estimated hydrodynamic boundary layer thicknesses.

Applying these concepts to other experimental explorations of the effects of ionic strength on colloid release showed that the use of ζ potentials as surface potentials has produced potential energy profiles with energy barriers for conditions that corresponded with observed rapid colloid release. With energy barriers present, the colloid release rate is predicted to be extremely slow; therefore, based on the results of this study, we suggest that rapid colloid release corresponds to conditions for which the energy barrier has vanished from the potential energy profile.

ACKNOWLEDGMENTS

We are grateful to François Morel, Keith Stolzenbach, and Menachem Elimelech for helpful discussions, to two anonymous reviewers for constructive criticisms of the manuscript, and to John MacFarlane for graphics. This research was supported by the Subsurface Science Program, Office of Health and Ecological Research, U.S. Department of Energy under Contract DE-FG02-89ER60846.

REFERENCES

1. Buddemeier, R. W., and Hunt, J. W., *Appl. Geochem.* **3,** 535 (1988).
2. Short, S. A., Lowson, L. T., and Ellis, J., *Geochim. Cosmochim. Acta* **52,** 2555 (1988).
3. Penrose, W. R., Polzer, W. L., Essington, E. H., Nelson, D. M., and Orlandini, K. A., *Environ. Sci. Technol.* **24,** 228 (1990).
4. Magaritz, M., Amiel, A. J., Ronen, D., and Wells, M. C., *J. Contam. Hydrol.* **5,** 333 (1990).
5. Langmuir, D., U.S. Geol. Survey Prof. Paper 650-C, C224 (1969).
6. Gschwend, P. G., and Reynolds, M. D., *J. Contam. Hydrol.* **1,** 309 (1987).
7. Degueldre, C., Baeyens, B., Goerlich, W., Riga, J., Verbist, J., and Stadelmann, P., *Geochim. Cosmochim. Acta* **53,** 603 (1989).
8. Gschwend, P. G., Backhus, D. A., MacFarlane, J. K., and Page, A. L., *J. Contam. Hydrol.* **6,** 307 (1990).
9. Ronen, D., Magaritz, M., Weber, U., Amiel, A., and Klein, E., *Water Resour. Res.* **28,** 1279 (1992).
10. Nightingale, H. I., and Bianchi, W. C., *Ground Water* **15,** 146 (1977).
11. Khilar, K. C., and Fogler, H. S., *J. Colloid Interface Sci.* **101,** 214 (1984).
12. Derjaguin, B. V., and Landau, L., *Acta Physicochim.* URSS **14,** 633 (1941).
13. Verwey, E. J. W., and Overbeek, J. Th. G., "Theory of the Stability of Lyophobic Colloids." Elsevier, Amsterdam, 1948.
14. Israelachvili, J. N., "Intermolecular and Surface Forces." Academic Press, New York, 1985.
15. Barouch, E., Matijević, E., and Wright, T. H., *Chem. Eng. Commun.* **55,** 29 (1987).
16. Dahneke, B., *J. Colloid Interface Sci.* **50,** 89 (1975).
17. Dahneke, B., *J. Colloid Interface Sci.* **50,** 194 (1975).
18. Ruckenstein, E., and Prieve, D. C., *AIChE J.* **22,** 276 (1976).
19. Hull, M., and Kitchener, J. A., *Trans. Faraday Soc.* **65,** 3093 (1969).
20. Bowen, B. D., and Epstein, N., *J. Colloid Interface Sci.* **72,** 81 (1979).
21. Gregory, J., and Wishart, A., *Colloids Surf.* **1,** 313 (1980).
22. Elimelich, M., *Water Research* **26,** 1 (1991).
23. Kallay, N., Barouch, E., and Matijević, E., *Adv. Colloid Interface Sci.* **27,** 1 (1987).
24. Ryan, J. N., and Gschwend, P. M., *Water Resour. Res.* **26,** 307 (1990).
25. Ryan, J. N., and Gschwend, P. M., *Geochim. Cosmochim. Acta* **56,** 1507 (1992).
26. Ryan, J. N., Ph.D. dissertation. Massachusetts Institute of Technology, Cambridge, MA.
27. Kallay, N., Biškup, B., Tomić, M., and Matijević, E., *J. Colloid Interface Sci.* **114,** 357 (1986).
28. Matijević, E., and Scheiner, P., *J. Colloid Interface Sci.* **63,** 509 (1978).
29. Hamaker, H. C., *Physica* **4,** 1058 (1937).
30. Israelachvili, J. N., and McGuiggan, P. M., *Science* **241,** 795 (1988).
31. Feke, D. L., Prabhu, N. D., Mann, J. A., Jr., and Mann, J. A., III, *J. Phys. Chem.* **88,** 5735 (1984).
32. Hogg, R., Healy, T. W., and Fuerstenau, D. W., *Trans. Faraday Soc.* **62,** 1638 (1966).
33. Gregory, J., *J. Colloid Interface Sci.* **51,** 44 (1975).
34. Lyklema, J., *Pure Appl. Chem.* **52,** 1221 (1980).
35. Hunter, R. J., "Zeta Potential in Colloid Science." Academic Press, New York, 1981.
36. van Oss, C. J., Chaudhury, M. K., and Good, R. J., *Chem. Rev.* **88,** 927 (1988).
37. Kallay, N., and Matijević, E., *Colloids Surfaces* **39,** 161 (1989).
38. Dzombak, D. A., and Morel, F. M. M., "Surface Complexation Modeling: Hydrous Ferric Oxide." Wiley–Interscience, New York, 1990.
39. Westall, J. C., Zachara, J. L., and Morel, F. M. M., "MINEQL: A Computer Program for the Calculation of Chemical Equilibrium Composition of Aqueous Systems." R. M. Parsons Laboratory Technical Note 18, Department of Civil Engineering, Massachusetts Institute of Technology, Cambridge, MA, 1976.
40. Parks, G. A., *Chem. Rev.* **65,** 177 (1965).
41. James, R. O., and Parks, G. A., *in* "Surface and Colloid Science" (E. Matijević, Ed.), Vol. 12, p. 119. Plenum, New York, 1982.
42. Schindler, P. W., and Gamsjager, H., *Kolloid Z. Z. Polym.* **250,** 759 (1972).
43. Henderson, D., and Lozada-Cassou, M., *J. Colloid Interface Sci.* **114,** 180 (1986).
44. Frens, G., and Overbeek, J. Th. G., *J. Colloid Interface Sci.* **38,** 376 (1972).

45. Kolakowski, J. E., and Matijević, E., *J. Chem. Soc. Faraday Trans. 1* **75,** 65 (1979).
46. Kuo, R. J., and Matijević, E., *J. Chem. Soc. Faraday Trans. 1* **75,** 2014 (1979).
47. Kuo, R. J., and Matijević, E., *J. Colloid Interface Sci.* **78,** 407 (1980).
48. Fitts, D. D., *Annu. Rev. Phys. Chem.* **17,** 59 (1966).
49. McDowell-Boyer, L. M., *Environ. Sci. Technol.* **26,** 586 (1992).
50. Levich, V. G., "Physicochemical Hydrodynamics." Prentice–Hall, Englewood Cliffs, NJ, 1962.
51. Clayfield, E. J., and Lumb, E. C., *Discuss. Faraday Soc.* **42,** 285 (1966).
52. Cerda, C., *Colloids Surf.* **27,** 219 (1987).
53. Hubbe, M. A., *Colloids Surf.* **16,** 249 (1985).
54. Sharma, M. M., Chamoun, H., Sita Rama Sarma, D. S. H., and Schechter, R. S., *J. Colloid Interface Sci.* **149,** 121 (1992).
55. Gotoh, K., Inoue, T., and Tagawa, M., *Colloid Polym. Sci.* **262,** 982 (1984).
56. Thompson, G., Kallay, N., and Matijević, E., *Chem. Eng. Sci.* **39,** 1271 (1984).
57. Kia, S. F., Fogler, H. S., and Reed, M. G., *J. Colloid Interface Sci.* **118,** 158 (1987).
58. Vaidya, R. N., and Fogler, H. S., *Colloids Surf.* **50,** 215 (1990).
59. Overbeek, J. Th. G., *Colloids Surf.* **51,** 61 (1990).
60. Israelachvili, J. N., and Adams, G. E., *J. Chem. Soc. Faraday Trans. 1* **74,** 975 (1978).
61. Kihira, H., and Matijević, E., *Adv. Colloid Interface Sci.* **42,** 1 (1992).